Fabrication and Characterization of Al/Ti/HfO_2/W Memristor-Based RF Switches

T. Amarilla, M. B. González, F. Campabadal, M. Nafria, *Senior Member, IEEE*, A. Crespo-Yepes, P. de Paco, *Senior Member, IEEE*, and J. Verdú, *Senior Member, IEEE*

***Abstract*—This work reports for the first time on the fabrication and the DC and radio frequency (RF) characterization of CMOS-compatible Al/Ti/HfO_2/W memristor-based RF switches, integrated with coplanar transmission lines (TLs) designs in two configurations: series and shunt memristor. The fabricated memristors show stable bipolar resistive switching and repeatable ON/OFF conductive states over multiple cycles, achieving an ON/OFF ratio exceeding one order of magnitude. During the memristor operation, increasing the current limit (CL) during SET process reduces the ON-state resistance, enhancing the conduction of the filament and improving the switch performance. The two RF switch configurations were also experimentally characterized in the frequency domain from 10 MHz to 50 GHz, revealing that CL controls the RF response of the switch: In the series configuration the insertion loss is reduced below 2.1 dB in the ON-state, whereas the shunt configuration achieves isolation up to 12 dB in the OFF-state. The cutoff frequency was extracted, reaching a value of 8.1 GHz. The experimental results demonstrate the potential of memristor devices as compact, low-power, nonvolatile RF switches, paving the way for their exploitation in RF applications and circuits.**

***Index Terms*—DC characterization, HfO_2, memristors, radio frequency (RF) measurements, resistive switch.**

I. Introduction

MEMRISTORS have attracted significant attention due to their potential for a wide range of applications [1], [2]. Among various materials, HfO_2-based memristors have emerged as particularly promising candidates due to their low operating voltage, thermodynamic stability, and nonvolatility [3], [4], [5]. The use of memristor devices in radio frequency (RF) systems has been subject to growing investigation [6], [7]. Notably, HfO_2 dielectrics have already been employed in the development of flexible RF switches [8], as well as in active mmWave components such as ferroelectric field-effect transistors (FeFETs) [9], further demonstrating the material's versatility across different device architectures. In addition, CMOS compatibility has already been demonstrated [10], [11]. Other devices used to develop RF switches, such as micro-electromechanical systems (MEMS)-based switches, offer excellent RF performance [12], [13], but typically require high operational voltages, exhibit slower switching times and high power consumptions, and are subject to packaging limitations due to their bulky structure [14]. Memristor-based RF switches, on the other hand, present a compelling alternative, leveraging their nonvolatility to reduce power consumption to maintain their resistive state [15], enabling more energy-efficient RF switching solutions.

In this letter, we demonstrate for the first time the fabrication and characterization of Al/Ti/HfO_2/W memristor-based switches integrated in a coplanar transmission line (TL) design in two configurations: series and shunt memristor, using a CMOS-compatible process. This work validates a new material stack suitable for CMOS integration and provides the first experimental assessment of its RF behavior in both configurations.

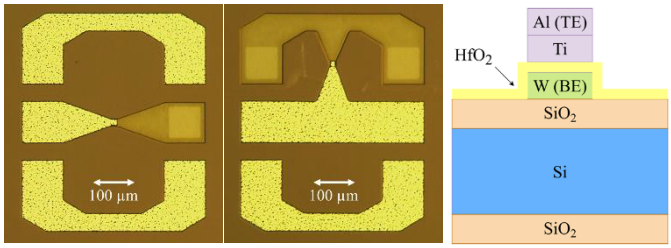

Fig. 1. Top-view optical microscope images of the fabricated devices: (a) series and (b) shunt configurations. (c) Cross-sectional view of the Al/Ti/HfO_2/W memristor stack.

II. Device Fabrication and Experimental Setup

The memristor-based RF switches were fabricated in both series and shunt configurations using a CMOS-compatible metal–insulator–metal (MIM) structure based on Al/Ti/HfO_2/W integrated in a coplanar TL design. Optical microscope images of the fabricated devices are shown in Fig. 1(a) for the series configuration and Fig. 1(b) for the shunt configuration. The cross-sectional view of the stack is also depicted in Fig. 1(c).

Received 18 March 2026; accepted 26 March 2026. Date of publication 14 April 2026; date of current version 4 September 2026. This work was supported in part by Spanish State Research Agency–Ministry of Science and Innovation under Project PID2024-159605OB-100, in part by the Department of Research and Universities of the Government of Catalonia under Project 2024 LLAV 00099, in part by the Instituto de Microelectrónica de Barcelona-Centro Nacional de Microelectrónica (IMB-CNM) through Ministerio de Ciencia, Innovación y Universidades/Agencia Estatal de Investigación (MICIU/AEI) and Fondo Europeo de Desarrollo Regional (FEDER) [European Union (EU)] under Project PID2022-139586NB-C42 and Project CNS2023-143898, in part by EU through the NextGenerationEU/Plan de Recuperación, Transformación y Resiliencia (PRTR) Program, and in part by the Consejo Superior de Investigaciones Científicas (CSIC) under Grant 2025ICT072. *(Corresponding author: T. Amarilla.)*

T. Amarilla, P. de Paco, and J. Verdú are with the Department of Telecommunications and Systems Engineering, Universitat Autònoma de Barcelona (UAB), 08193 Cerdanyola del Vallès, Spain (e-mail: tobias.amarilla@autonoma.cat).

M. B. González and F. Campabadal are with the Institut de Microelectrònica de Barcelona (IMB-CNM-CSIC), 08193 Cerdanyola del Vallès, Spain.

M. Nafria and A. Crespo-Yepes are with the Department of Electronic Engineering, Universitat Autònoma de Barcelona (UAB), 08193 Cerdanyola del Vallès, Spain.

Digital Object Identifier 10.1109/LMWT.2026.3678995

© 2026 The Authors. This work is licensed under a Creative Commons Attribution 4.0 License.
For more information, see https://creativecommons.org/licenses/by/4.0/

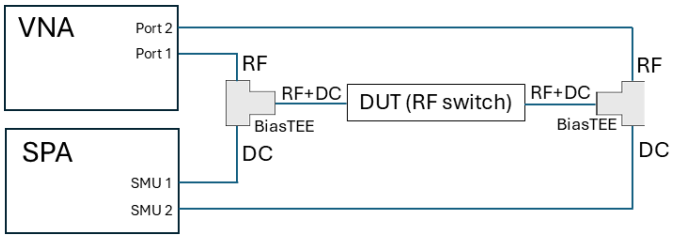

Fig. 2. Measurement setup for DC and RF characterization.

Fabrication was carried out on high-resistivity silicon substrates (>30 kΩ·cm, 800 μm thick), thermally oxidized to grow a 1-μm-thick SiO_2 insulating layer. A 200-nm-thick tungsten (W) bottom electrode (BE) was deposited by magnetron sputtering and patterned using maskless direct laser lithography followed by wet etching. A 10-nm-thick HfO_2 switching layer was then deposited by atomic layer deposition (ALD) at 225 °C, using tetrakis(dimethylamido)-hafnium (TDMAH) and H_2O as precursors, with N_2 serving as both carrier and purge gas.

The top electrode (TE), which consisted of a bilayer comprising a 12-nm-thick titanium (Ti) layer and a 1.5-μm-thick aluminum (Al) layer, was deposited by magnetron sputtering and patterned by maskless direct laser lithography and wet etching.

After metallization, a third lithography step was performed to open vias through the HfO_2 layer, enabling electrical contact to the W BE.

The DC and RF characterization were performed using a Keithley 4200 SPA and Keysight Streamline P5008A VNA. As shown in Fig. 2, bias-tees were employed to couple the instruments to the device GSG probes, allowing simultaneous DC biasing and RF signal transmission without reconfiguration.

III. Memristor-Based RF Switches Characterization

A. DC Characterization

The DC characterization of the memristors has been carried out applying positive voltage ramps (from 0 to +1 V) for SET operations, and negative ramps for RESET (from 0 to −1.2 V). During SET, a current limit (CL) from 1 to 3 mA was applied, whereas no CL was applied during RESET to ensure the correct cycling sequence. Fig. 3(a) shows the *I–V* curves obtained over 130 cycles for a shunt configuration device with an active area of 16.52 μm^2. The memristor exhibits stable and repeatable bipolar resistive switching, with a clear distinction between the low-resistance state (LRS) and the high-resistance state (HRS), and an ON-/OFF-state ratio greater than one order of magnitude [Fig. 3(b)]. Furthermore, the cycle-to-cycle variability was evaluated using a Weibull statistical distribution [Fig. 3(c)], confirming the stability of the absolute currents across all cycles. Moreover, the LRS resistance can be reduced by increasing the CL during SET, as demonstrated in Fig. 3(a) where CL is increased from 1 to 3 mA after 30 cycles. The HRS current remains approximately constant regardless of the CL, resulting in an improved ON/OFF ratio at higher CLs.

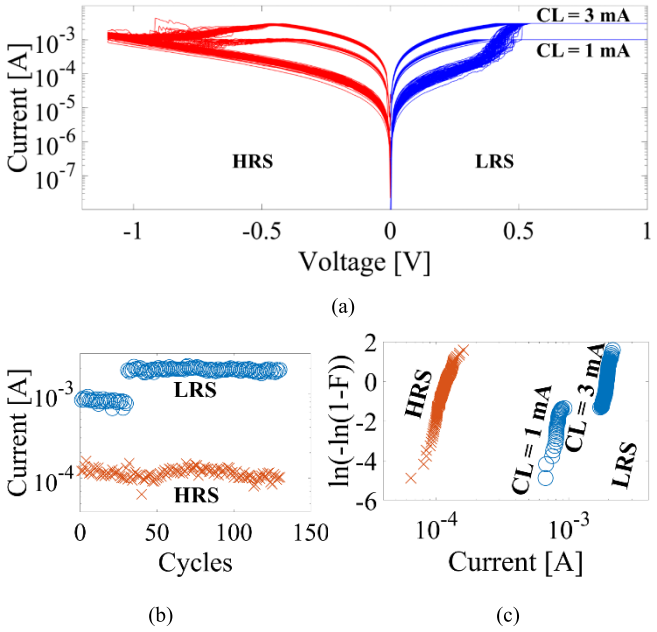

Fig. 3. (a) Memristor *I–V* curves over 130 switching cycles. (b) LRS/HRS resistive states over the measured cycles. (c) Weibull statistical distribution of the LRS/HRS state currents.

B. RF Characterization

RF measurements were conducted after the SET or RESET DC processes, with the devices held at 0-V bias to ensure stable and consistent DC conditions. We observed that although the forming process performed with low CL values (1–3 mA) produced a CF capable of delivering an initial RF performance comparable to that obtained with higher CLs, these current levels were insufficient to reliably reform a low-resistance filament in subsequent SET cycles, leading to partial or incomplete filament reconstruction.

For this reason, the RF characterization was carried out using higher CL values (5–45 mA), which enabled more reproducible filament formation from cycle to cycle and resulted in a substantial improvement in RF performance.

Importantly, the devices consistently returned to the HRS after each RESET operation, without degradation or permanent damage. RF measurements were performed from 10 MHz to 50 GHz, and the results are presented on a logarithmic frequency scale to highlight the low-frequency state transitions.

1) Series Switch Configuration: In the series configuration, the memristor controls the transmission path between the input and output ports. The RF switch operates in the ON-state when the memristor is in LRS, allowing signal propagation through the line. Conversely, the switch operates in the OFF-state when the memristor is in HRS, effectively blocking signal transmission. The measured RF responses are shown in Fig. 4. For the ON-state [Fig. 4(a)], increasing CL during SET significantly reduces insertion loss, reaching values from below 2.1 dB up to 50 GHz for CL = 45 mA. This behavior is consistent with the DC analysis, where higher CL produces more conductive filaments, reducing the memristor resistance and thereby enhancing RF transmission.

For the OFF-state [Fig. 4(b)], isolation ranges between 10 and 15 dB up to approximately 0.5 GHz. Unlike the

TABLE I
COMPARISON OF THIS WORK WITH OTHER REPRESENTATIVE RF SWITCHES

Reference	Device Technology	Non-volatility	Control Voltage	Cutoff freq. (Hz)	Freq. (GHz)	IL (dB)	ISO (dB)	Active Area (μm^2)	Max. Power (dBm)
This work	**HfO_2**	**Yes**	**0.5 ~ 1 / -0.5~-0.9 V**	**8.1 G**	**dc - 50**	**< 2.1**	**≥ 10 (≤ 0.5 GHz)**	**16.52**	**21**
[16]	hBN	Yes	-1 / 1.5 V	43 T	dc- 110	≤ 0.2	≥ 15	0.05	20
[17]	MoS_2	Yes	-0.7 / 1.4 V	11 T	dc - 50	~ 0.3	> 20	0.125	11
[18]	MEMS	No	75~80 V	5 T	dc - 40	< 1	> 30	120x160	>36
[19]	VO_2 PCM	No	2.2 V @ 45 mA	3.8 T	dc - 60	< 0.4	> 25	150	29
[20]	GeTe PCM	Yes	5.6 / 12.7 V	1.7 T	dc - 6	≤ 0.3	> 15	356	37

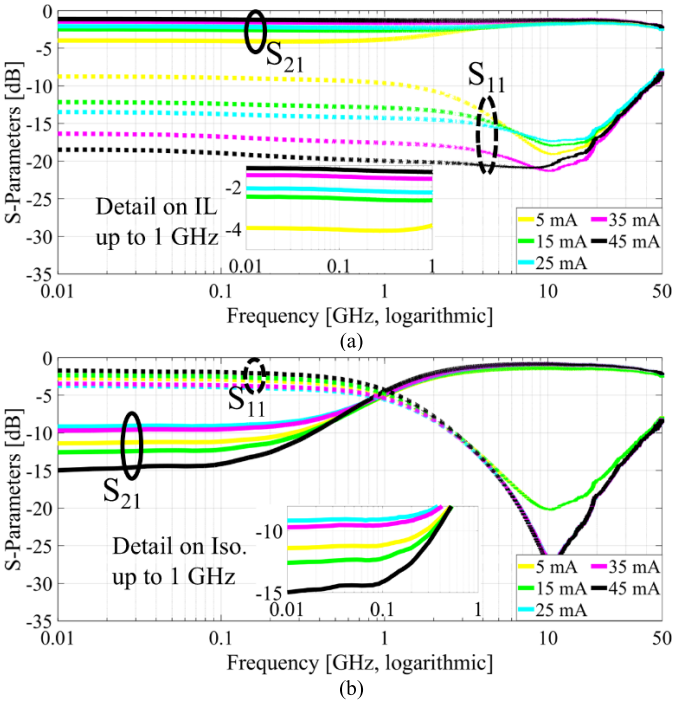

Fig. 4. RF response of the series RF switch for different CL values. (a) Memristor in LRS. (b) Memristor in HRS.

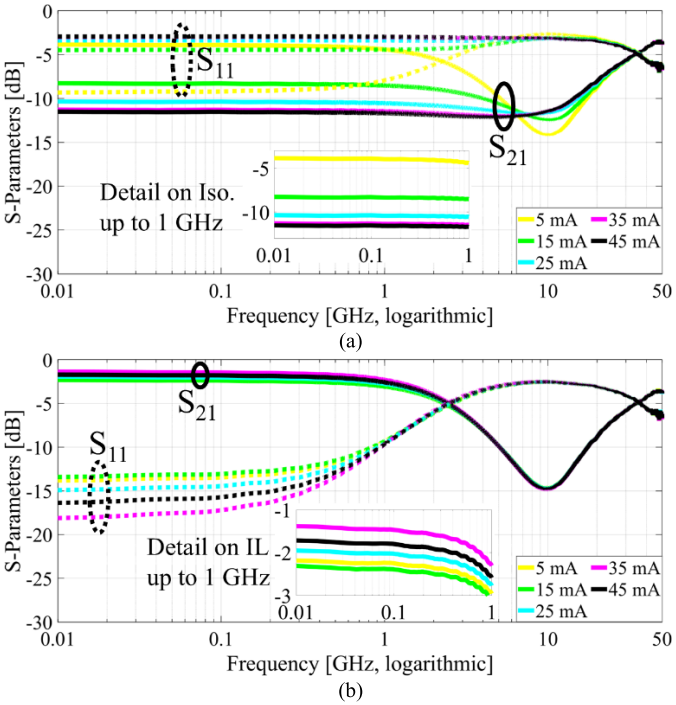

Fig. 5. RF response of the shunt RF switch for different CL values. (a) Memristor in LRS. (b) Memristor in HRS.

ON-state, the OFF-state response does not depend on CL during SET process, exhibiting stochastic behavior according to the intrinsic variability of the memristor switching dynamics phenomenon [21]. However, the experimental results evidence a frequency limitation in this configuration, with effective operation restricted to 0.5 GHz.

2) Shunt Switch Configuration: In the shunt configuration, the memristor connects the TL between the input/output ports and the ground. The RF switch operates in the OFF-state when the memristor is in LRS, diverting the signal to ground. Conversely, the switch operates in the ON-state when the memristor is in HRS, allowing the RF signal to propagate through the input/output ports. The measured RF responses are shown in Fig. 5. For the memristor in LRS [Fig. 5(a)], increasing CL during SET improves isolation, from about 4 to 12 dB up to 8 GHz. Higher CL values promote the formation of more robust and conductive filaments, as confirmed in Sections III-A and III-B1. This configuration exhibits a wider isolation bandwidth because it relies on the frequency-independent low-resistance path to ground, unlike capacitive coupling limiting the series switch.

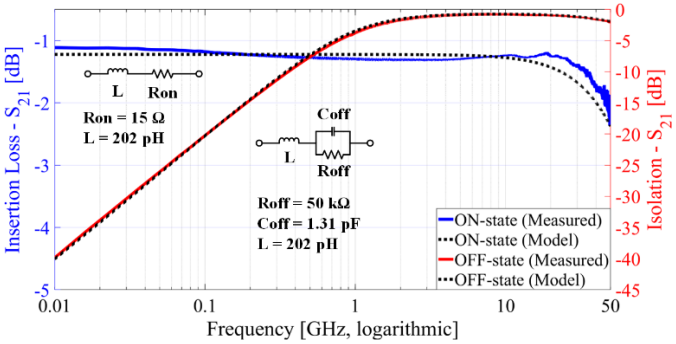

Fig. 6. Measured S_{21} magnitude of the series RF switch in the ON-state (blue) and OFF-state (red), compared with the corresponding equivalent circuit model (dotted black).

For the memristor in HRS [Fig. 5(b)], the response is independent of CL, consistent with intrinsic RESET behavior. Insertion loss remains close to 2 dB for all cases up to 1 GHz, indicating that in RESET operations, the shunt configuration exhibits lower variability compared to the series configuration. Moreover, the shunt configuration switch exhibits an extended frequency response, maintaining functionality up to 1 GHz, compared to 0.5 GHz in the series configuration.

3) Cutoff Frequency Analysis: The cutoff frequency (F_c) was extracted by fitting the measured S_{21} to the equivalent circuit model (Fig. 6). The ON-state is represented by a series R_{on} and a parasitic inductance L, while the OFF-state includes a parallel C_{off}–R_{off} network, in series with L. Extracting R_{on} = 15 Ω, R_{off} = 50 kΩ, C_{off} = 1.31 pF, and L = 202 pH, yields an $F_c = 1/(2\pi R_{on} C_{off})$ of 8.1 GHz.

The currently measured F_c is primarily limited by the large active area, given that C_{off} scales with $\varepsilon_r \varepsilon_0 A/d$. While increasing the HfO_2 thickness (d) would reduce capacitance, it would undesirably increase the forming and operating voltages. Consequently, minimizing the active area (A) emerges as the dominant strategy to maximize F_c, currently limited by the photolithography resolution. Since the conduction is filamentary, the required CL depends on the filament properties rather than the total device area; thus, scaling down will not degrade the ON-state resistance. To validate the intrinsic potential of the technology, electromagnetic simulations were performed on a geometrically optimized structure, reducing the active area to 0.125 μm^2 (comparable to MoS_2 switches [17]), yielding a projected F_c exceeding 1 THz. Additionally, these simulations indicate that increasing the thickness of the W BE significantly reduces conductor losses, further improving insertion loss and isolation.

Table I compares this work with state-of-the-art switching technologies. Although the current active area limits the F_c, the proposed HfO_2 device offers critical advantages for high-density integration. Specifically, it features a compact footprint significantly smaller than standard MEMS or PCM devices, combined with low actuation voltages and nonvolatile state retention with zero static power consumption. Finally, the fully CMOS-compatible process significantly simplifies fabrication.

IV. Conclusion

This work demonstrated the first CMOS-compatible Al/Ti/HfO_2/W memristor RF switches in series and shunt configurations. The devices exhibit stable, nonvolatile resistive switching for reliable RF signal control. The series switch operates up to 0.5 GHz (2.1-dB insertion loss, >10-dB isolation), while the shunt configuration extends functionality up to 1 GHz (12-dB isolation, 2-dB insertion loss), offering higher robustness and repeatability. In both geometries, RF performance is strictly governed by the CL applied during SET. These results also highlight that the memristor active area fundamentally limits the maximum operating frequency.

References

[1] L. Chua, "Memristor–the missing circuit element," *IEEE Trans. Circuit Theory*, vol. CT-18, no. 5, pp. 507–519, Sep. 1971, doi: 10.1109/TCT.1971.1083337.

[2] D. B. Strukov, G. S. Snider, D. R. Stewart, and R. S. Williams, "The missing memristor found," *Nature*, vol. 453, no. 7191, pp. 80–83, May 2008, doi: 10.1038/nature06932.

[3] H. Abunahla, B. Mohammad, M. A. Jaoude, and M. Al-Qutayri, "Novel hafnium oxide memristor device: Switching behaviour and size effect," in *Proc. IEEE Int. Symp. Circuits Syst. (ISCAS)*, Baltimore, MD, USA, May 2017, pp. 1–4, doi: 10.1109/ISCAS.2017.8050791.

[4] M. B. González et al., "Analysis of the characteristic current fluctuations in the high resistance state of HfO2-based memristors," in *Proc. 13th Spanish Conf. Electron Devices (CDE)*, Jun. 2021, pp. 8–11, doi: 10.1109/CDE52135.2021.9455725.

[5] R. Rodriguez et al., "Beneficial role of noise in hf-based memristors," in *Proc. IEEE Int. Symp. Circuits Syst. (ISCAS)*, Austin, TX, USA, May 2022, pp. 975–979, doi: 10.1109/ISCAS48785.2022.9937850.

[6] E. Tsipas et al., "Modeling of memristor-based RF switches," in *Proc. 12th Int. Conf. Modern Circuits Syst. Technol. (MOCAST)*, Athens, Greece, Jun. 2023, pp. 1–4, doi: 10.1109/MOCAST57943.2023.10177033.

[7] Q. Xia, "Memristive nanodevices: CMOS compatibility and novel applications," in *Proc. 18th Medit. Electrotechnical Conf. (MELECON)*, Lemesos, Cyprus, Apr. 2016, pp. 1–4, doi: 10.1109/MELCON.2016.7495316.

[8] S.-C. Chen et al., "HfO2 memristor-based flexible radio frequency switches," *ACS Nano*, vol. 19, no. 1, pp. 704–711, Jan. 2025, doi: 10.1021/acsnano.4c11846.

[9] S. Abdulazhanov et al., "Reconfigurable ferroelectric hafnium oxide FeFET fabricated in 28 nm CMOS technology for mmWave applications," in *Proc. ESSDERC - IEEE 53rd Eur. Solid-State Device Res. Conf. (ESSDERC)*, Lisbon, Portugal, Sep. 2023, pp. 113–116, doi: 10.1109/ESSDERC59256.2023.10268544.

[10] Q. Xia et al., "Memristor–CMOS hybrid integrated circuits for reconfigurable logic," *Nano Lett.*, vol. 9, no. 10, pp. 3640–3645, Oct. 2009, doi: 10.1021/nl901874j.

[11] S. Pi, P. Lin, H. Jiang, C. Li, and Q. Xia, "Device engineering and CMOS integration of nanoscale memristors," in *Proc. IEEE Int. Symp. Circuits Syst. (ISCAS)*, Melbourne, VIC, Australia, Jun. 2014, pp. 425–427, doi: 10.1109/ISCAS.2014.6865156.

[12] J. Iannacci, M. Huhn, C. Tschoban, and H. Pötter, "RF-MEMS technology for 5G: Series and shunt attenuator modules demonstrated up to 110 GHz," *IEEE Electron Device Lett.*, vol. 37, no. 10, pp. 1336–1339, Oct. 2016, doi: 10.1109/LED.2016.2604426.

[13] X. Gao, L. Han, M. Nie, and Q. Huang, "The study of a RF MEMS switch based on LCP substrate," in *Proc. IEEE Sensors*, Jun. 2015, pp. 1–4, doi: 10.1109/ICSENS.2015.7370440.

[14] J. Verdu, T. Amarilla, Y. Shen, S. Pazos, M. Lanza, and P. de Paco, "Characterization of nonvolatile switches based on 2-D multilayered hBN memristors for high-frequency applications," *IEEE Microw. Wireless Technol. Lett.*, vol. 35, no. 9, pp. 1380–1383, Sep. 2025, doi: 10.1109/LMWT.2025.3576996.

[15] S. Pazos et al., "Memristive circuits based on multilayer hexagonal boron nitride for millimetre-wave radiofrequency applications," *Nature Electron.*, vol. 7, no. 7, pp. 557–566, Jul. 2024, doi: 10.1038/s41928-024-01192-2.

[16] M. Kim et al., "Non-volatile RF and mm-wave switches based on monolayer hBN," in *IEDM Tech. Dig.*, San Francisco, CA, USA, Dec. 2019, pp. 1–4, doi: 10.1109/IEDM19573.2019.8993470.

[17] M. Kim et al., "Zero-static power radio-frequency switches based on MoS_2 atomristors," *Nature Commun.*, vol. 9, no. 1, Jun. 2018, Art. no. 2524, doi: 10.1038/s41467-018-04934-x.

[18] C. D. Patel and G. M. Rebeiz, "A compact RF MEMS metal-contact switch and switching networks," *IEEE Microw. Wireless Compon. Lett.*, vol. 22, no. 12, pp. 642–644, Dec. 2012, doi: 10.1109/LMWC.2012.2226637.

[19] T. G. Williamson and N. Ghalichechian, "Novel high speed PCM switch based on vanadium dioxide with less than 500 ns switching time," *IEEE Microw. Wireless Technol. Lett.*, vol. 36, no. 1, pp. 79–82, Jan. 2026, doi: 10.1109/LMWT.2025.3611674.

[20] I. Charlet et al., "RF performance of large germanium telluride switches for power application," in *Proc. 18th Eur. Microw. Integr. Circuits Conf. (EuMIC)*, Sep. 2023, pp. 177–180, doi: 10.23919/EUMIC58042.2023.10288974.

[21] P. Trousset et al., "Fabrication and characterization of MoS_2-based RF memristor switches for terahertz applications," in *Proc. 54th Eur. Microw. Conf. (EuMC)*, Paris, France, Sep. 2024, pp. 776–779, doi: 10.23919/eumc61614.2024.10732829.